Characterization and comparison of natural and Zachery-treated turquoise: new data

Valeria Diella[1*], Marco Cantaluppi[2], Rosangela Bocchio[2], Elena Possenti[3], Ilaria Adamo[4], Giancarlo Della Ventura [5], Lucia Mancini[6], Nicoletta Marinoni[2]

[1] National Research Council, Institute of Environmental Geology and Geoengineering (IGAG), Section of Milan, via Botticelli 23, 20133 Milan, Italy; valeria.diella55@gmail.com, *Orcid ID*: 0000-0001-8767-9164

[2] Department of Earth Sciences "Ardito Desio", University of Milan, via Botticelli 23, 20133 Milan, Italy; marco.cantaluppi@unimi.it, Orcid ID: 0000-0002-3914-6491; rosangela.bocchio@unimi.it, *Orcid ID*: 0000-0002-8635-0874; nicoletta.marinoni@unimi.it, *Orcid ID*: 0000-0003-4969-4923

[3] National Research Council, Institute of Heritage Science (ISPC), Section of Milan, Via R. Cozzi 53, 20125 Milan, Italy; elena.possenti@cnr.it; *Orcid ID*: 0000-0002-9041-7971

[4] Italian Gemmological Institute (IGI), Piazza S. Sepolcro 1, 20123 Milan, Italy; ilaria.adamo@igi.it

[5] Department of Sciences, University of Rome Tre, Largo S. Leonardo Murialdo 1, 00146 Rome, Italy; giancarlo.dellaventura@uniroma3.it, *Orcid ID*: 0000-0001-6277-961X

[6] Elettra-Sincrotrone Trieste S.C.p.A., s.s. 14 km 163,500 in Area Science Park, 34149 Basovizza (Trieste), Italy; lucia.mancini@elettra.eu

*Correspondence: valeria.diella55@gmail.com

Abstract Turquoise is a well-known gemstone that has been used in artefacts across many cultures throughout history. However, due to its porosity it is often treated to enhance its color and beauty. One appreciated treatment is the patented Zachery process, although its details remain publicly undisclosed. Previous studies indicated that only a high K content distinguishes Zachery-treated from natural turquoises. In this study, natural and Zachery-treated turquoise samples from the famous Kingman mine, Arizona, USA, were analysed by means a multi-methodological approach, including standard gemological testing, electron microprobe (EMPA), scanning electron microscope with energy dispersive spectrometer (SEM-EDS) and X-ray diffraction (XRD), Fourier-Transform InfraRed (FTIR), non-destructive External Reflection-Fourier-Transform InfraRed (ER-FTIR) spectroscopy and X-ray computed microtomography (μCT). The results revealed new chemical-mineralogical and microstructural features that distinguish the Zackery-treated from the natural turquoise: higher specific gravity and lower porosity, associated to a high and uneven concentrations of Cu, K and Na, the occurrence of tenorite (CuO), the presence and extension of reaction edges in the entire volume are distinctive of treated samples. Moreover, Cu-rich seeds and feldspar crystals may be interpreted as additional components used during the treatment. The hypothesis is that the Zachery treatment induces the re-crystallization of a new turquoise-like phase, which differs from the natural one from a chemical and microstructural point of view.

Keywords: turquoise, gemology, Zachery method, FTIR and ER-FTIR spectroscopy, chemical analyses, X-ray computed microtomography

Introduction

The main purpose of the activity of gemologists is the evaluation of gem materials, that is establishing their identity and determining whether they are natural or synthetic and/or if they have been treated (Fritsch and Rondeau 2009). The term "*Treatment*" refers to any artificial process, different from cut and assembly, used to improve the gem color, appearance, and durability. All stones, even artificial ones, can be subjected to treatments, which must be explicitly declared as such (Shigley and McClure 2009). In the past, some treatments were not disclosed but generally accepted; one example is the fracture filling with oil of emerald, a treatment that is no longer accepted unless it is disclosed. Turquoise, with chemical formula $CuAl_6(PO_4)_4(OH)_8 \cdot 4H_2O$, is one of the first gem materials that has been subjected to various methods of treatments to improve its appearance and mechanical properties and consequently to increase the amount available and its commercial value. The ancient use of turquoise in jewelry dates back to the beginning of civilization, from ancient Persia (7000 B.C.) and Egypt (5000 B.C.) to present day (Hole et al. 1969; Carò et al. 2021 and references therein). Turquoise occurs in dry and barren regions where acidic, copper-rich groundwater reacts with minerals containing phosphorous and aluminium and is found in large amounts in Iran, China, Mexico, Australia and in south western part of USA, mainly in Nevada and Arizona (Schwarzinger and Schwarzinger 2017 and reference therein). However, in most cases, the sources of high-quality gem samples are limited and unsatisfactory for the demand of the market. Moreover, turquoise, being a cryptocrystalline aggregate with various degrees of porosity, can easily accept many treatments. The most common type of turquoise treatment is the impregnation with organic material, such as polymers and wax, which improves the durability and appearance of the gemstone (Fritsch et al. 1999; McClure et al. 2010). The distinction of natural, untreated turquoise from its counterpart by impregnation requires a combination of standard gemological observations with more sophisticated techniques, mainly Raman and Fourier-transform infrared (FTIR) spectroscopy, chemical analyses, X-ray diffraction, and analytical pyrolysis (Lind et al. 1983; Fritsch et al. 1999; McClure et al. 2010; Čejka et al. 2015; Schwarzinger and Schwarzinger 2017; Sabbaghi 2018; Dumanska-Slowik et al. 2019).

Since 1988, a new proprietary type of turquoise treatment, called "Zachery treatment" has appeared on the market (Fritsch et al. 1999 and references therein). The treatment greatly enhances the stone quality and aspect preserving its gemological properties, decreasing its porosity, improving its color, and allowing easier polishing. Fritsch et al. (1999) published a thorough paper on this proprietary process highlighting the difficulties to recognize the treated turquoises by standard gemological techniques and assessing that this treatment does not involve any impregnation with a polymer. In that paper, the Zachery method is described as a process involving a bath of mineral fragments under a flux of electrical current. Fritsch et al. (1999) claimed that the enhancement process is based on the attempts to duplicate the environment that allowed the famous Kingman high-grade turquoise to be deposited amid large potassium feldspar beds and that the procedure, including the electrodes controlling the current flux, did not contain colouring ions such as iron and copper. The Authors concluded that only the exposition to oxalic acid that bleach the stone or chemical analysis that detects the presence of potassium, found in most Zachery-treated turquoises, may identify the treatment. Further studies on Zachery-treated turquoises (Kwon et al. 2009; Sun et al. 2014) reiterated that only the high content of potassium could be used to distinguish natural from treated stones.

The present study characterizes and compares natural and Zachery-treated turquoise by a multidisciplinary approach combining either non-destructive or invasive methods. The research has a dual purpose: first to clarify the Zachery treatment, which is still undisclosed and, second, to provide distinctive features that facilitate the easy and rapid recognition of treated samples.

The non-destructive techniques on cut samples, regardless their size, include gemological investigation, External Reflection-Fourier-Transform InfraRed (ER-FTIR) spectroscopy, and X-ray computed microtomography (μCT) whereas chemical analyses by Electron Microprobe (SEMQ), scanning electron microscope with energy dispersive spectrometer (SEM-EDS), analyses by X-ray diffraction (XRD) and Fourier-Transform InfraRed (FTIR) spectroscopy imply loss or damage of the samples.

Materials and Methods

A group of thirty-one gem-quality turquoises from the Kingman mine (Arizona, USA), fourteen natural and seventeen Zachery-treated, provided by the Italian Gemological Institute (IGI) thanks to Dr. Claudio Cimmino, Bangkok, Thailandia, were investigated using different techniques to characterize their morphological and chemical features. In the following, *TN* and *TT* will refer to natural and treated turquoises, respectively.

Five natural (*TN_1-5*) and six treated (*TT_1-6*) gems were tested by standard gemological methods at the Italian Gemological Institute of Milan (Italy) to determine their gemological properties. Three treated samples (*TT_1-3*) were sawed in half to investigate their cross sections. The samples weighing from 1.51 to 7.87 ct are fashioned as cabochons or spheres. Their refractive index, n, was measured by the spot method with a Krüss refractometer (A. Krüss Optronic, Hamburg, Germany) using ordinary light source with a sodium filter (wavelength λ = 589 nm) and methylene iodide as a contact liquid (n = 1.80). A Mettler hydrostatic balance was used to determine the specific gravity (SG) in bi-distilled water. We also examined the reaction of the samples to both the long-wave (λ = 366 nm) and short-wave (λ = 245 nm) ultraviolet radiation in a darkened room. Moreover, a Motic GM168 dark-field gemological microscope was used for the microscopic observations.

Quantitative chemical analyses of major and minor elements were performed and backscattered electron (BSE) images acquired on the polished surface of three natural specimens (*TN_6*, *TN_7* and *TN_8*), on the polished surface of a treated one (*TT_7*) and on two perpendicularly cut treated specimens (*TT_8* and *TT_9*) using the JEOL JXA-8200 electron microprobe in wavelength dispersion mode (EMPA–WDS) at the Department of Earth Sciences of the University of Milan, Italy. The system was operated with an accelerating voltage of 15 kV, 5 nA beam current and a counting time of 60 s on the peak and 30 s on the background selecting 10 μm diameter spot to prevent the sample sublimation under the electron beam. Natural minerals were used as standards and the rough data were corrected for matrix effects using a conventional ΦρZ routine in the JEOL software package.

At the same laboratories, a further investigation was performed using the Scanning Electron Microscope (SEM) JSM-IT 500 (JEOL, 2019), equipped with an Energy Dispersive Spectrometer (EDS), to obtain X-ray maps, secondary and backscattered electron (SE and BSE) images at high magnification and rapid semi-quantitative analyses. Twelve samples, 2 natural (*TN_9-10*) and 10 treated (*TT_10-19*), have been coated with gold for secondary electron images or carbon for BSE images, semi-quantitative chemical analyses, and X-ray maps.

Five fragments (two natural, *TN_12-13*, and three treated, *TT_21-23*) were selected for powder X-ray diffraction measurements. The analyses were performed at the Department of Earth Sciences of the University of Milan, Italy, by a Panalytical X'Pert-PROMPD X'Celerator X-ray powder diffractometer, using Cu Kα radiation (λ = 1.5418 Å), at a beam voltage of 40 kV and a current of 40 mA. X-ray powder diffraction patterns were collected over the 9–120° range of the scattering angle 2θ, with steps of 0.01° 2θ and a count time of 50 s per step. The lattice parameters of the turquoise samples were determined by using Si (NBS SRM 640b) as an internal standard and the General Structure Analysis System (GSAS) software was used to process XRD data (Rietveld 1969; Toby and Dreele 2013).

Infrared spectroscopy measurements were carried out on natural and treated turquoises with two different instrumental setups (powder FTIR and External Reflection FTIR) described below. The aim was to explore the vibrational features of the gems and the potentials of the two IR approaches in detecting the differences between the natural and treated turquoises. External reflection FTIR is a relatively little-exploited but efficient method to identify minerals and gems (Hainschwang and Notari, 2008).

The Powder FTIR spectra were collected at the laboratory of Department of Sciences, University of Rome Tre, Italy, on one natural (*TN_14*) and three treated (*TT_24-26*) turquoises using a Nicolet iS50 FTIR spectrometer equipped with a DTGS detector and a KBr beam splitter in a spectral rage of 4000-400 cm^{-1}; the nominal resolution was 4 cm^{-1} and 64 scans were averaged for both samples and background. Small fragments were manually extracted under the binocular microscope from the pristine and treated turquoise, respectively, based on the different blue hue of the sample and the distance from the rim of the gemstone, that was affected by the treatment. The fragments were ground using an agate mortar, mixed with KBr (mineral:KBr ratio = 1:200 mg) and pressed to prepare the conventional KBr disks for IR transmission analysis.

External reflection Fourier transform infrared spectroscopy (ER-FTIR) measurements were carried out on one natural (*TN_15)* and two treated turquoises (*TT_20* and *TT_27*) using a Thermo Scientific™ Nicolet™ iS50 FT-IR spectrophotometer coupled with a Continuum™ infrared microscope equipped with a mercury cadmium telluride (MCT/A) detector cooled with liquid nitrogen and located at the laboratory of the Institute of Heritage Science (ISPC-CNR), Milan, Italy. The investigations were performed non-invasively in specular reflectance geometry, in the spectral range 4000–650 cm^{-1}, with a 4 cm^{-1} resolution and by merging 128 co-added scans. The background spectra were collected on a golden mirror. The investigated area was 100 × 100 μm^2 for each ER-FTIR spectrum. ER-FTIR measurements were done on the external surface of the gems and along traverse from rim to centre. In the following, the ER-FTIR spectra are presented in reflectance without any spectral manipulation or spectral conversion.

Laboratory-based X-ray computed microtomography (μCT) analyses of two cut turquoises, one natural (*TN_11*) and one treated (*TT_20*), were performed at the TomoLab station (Mancini et al. 2007; Zandomeneghi et al. 2010; Kudrna Prašek et al. 2018; Caruso et al. 2020) of the Elettra synchrotron facility in Basovizza (Trieste, Italy). This μCT system is equipped with a sealed microfocus X-ray source (L9181, Hamamatsu Photonic, Japan) operating in a Voltage range of 40 -130 kV with a maximum power of 39 W, a minimum focal spot size of 5 μm and delivering an X-ray beam with a cone beam geometry. The detector used was a 12-bit, water-cooled, full frame CCD camera (4008 x 2672 pixels) coupled to a Gadox scintillator screen by a fiber-optic taper. This camera has an effective pixel size of 12.5x12.5 mm^2 corresponding to a maximum field of view of 50 x 33 mm^2. The experimental parameters used for the tomographic scans are the followings: Voltage = 130 kV, current = 61 μA, angular step = 0.2°, total scan angle = 360°, scan duration = 174 min, scaled pixel size = 5 μm). The slice reconstruction was carried out using the free software Necon 1.7 (Bruker, USA) based on the Feldkamp algorithm (Feldkamp et al. 1984), which also allows us to correct beam hardening and ring artefacts. The visualization of the reconstructed virtual section of the samples was obtained by the freeware ImageJ, while for the 3D visualization (rendering) of the virtual volumes, the commercial software VGStudio Max 2.0 (Volume Graphics, Germany) was applied.

Image segmentation, aimed at extracting the pores/cracks from the matrix, has been performed by manual 3D Otsu thresholding using the Fijii software (Schindelin et al. 2012) and the results are reported as pore volume percentage (%. vol).

Results

Gemological properties

The samples range in color from whitish or greenish light blue to dark blue. In general, the treated samples have darker and more saturated colors, unnatural in appearance, when compared with their untreated counterparts, which appear whitish or greenish light blue in color. Moreover, the luster of the treated stones is better than of untreated samples which show a chalky luster (Fig. 1).

For all samples the refractive index ranges from 1.60 to 1.62 (spot method), in agreement with literature data (Fritsch et al. 1999). The measured specific gravity (SG) of natural untreated stones ranges from 2.44 to 2.57 g/cm^3 and increases from about 5 up to 15% after about a quarter of an hour immersed in water. The treated samples have no tendency to absorb water and their SG results in the range from 2.65 to 2.74 g/cm^3. This confirms that the untreated turquoise samples are more porous than their treated counterparts.

All samples (both untreated and treated) are inert to short-wave UV and show a weak to very weak whitish blue or whitish green luminescence to long-wave irradiation. When viewed with the gemological microscope, all untreated samples reveal a typical turquoise structure with cavities, whitish spots and yellow inclusions having metallic luster (pyrite). The treated samples are more homogeneous in their appearance and show, in the half-sawed ones, a rim of more saturated blue color that can already be seen with a naked eye. Some treated samples show a concentration of color along the fractures, not only confined to the fracture itself (as in the case of dyed samples) but also expanding on either side of the break. This color concentration, as well as the gem color itself, is rather unnatural to our experience and resulting from a treatment to improve the color in agreement with Fritsch et al. (1999).

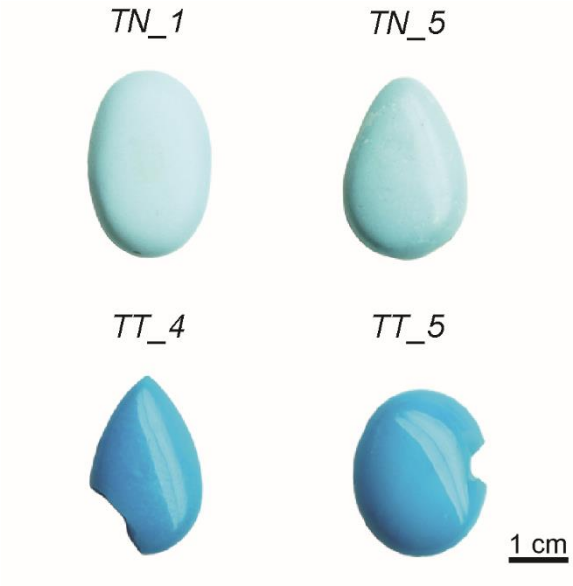

Fig. 1 Examples of studied turquoises: *TN_1*: 11.18x17.43x5.22 mm, 7.867 ct; *TN_5*: 9.89x13.61x4.39 mm, 4.29 ct; *TT_4*: 7.87x13.18x2.44 mm, 1.67 ct; *TT_5*: 7.89x10x2.76 mm, 1.508 ct. Photos by Ludovica Faldi

Chemical analyses

The chemical analyses of natural and treated samples were performed on several points and lines from rim to center or from rim to rim. In natural gems, the compositions of different points resulted very similar and in agreement with the stoichiometric formula of turquoise (Table 1). As usual in turquoise matrix, pyrite and kaolinite have been detected as accessory minerals.

Table 1 Electron microprobe analyses of natural turquoises

Sample	*TN_6*		*TN_7*		*TN_8*	
	Average 31 pts	st dev	Average 31 pts	st dev	Average 31 pts	st dev
P_2O_5 (wt%)	33.61	0.48	34.31	0.45	33.78	0.55
SiO_2	0.01	0.02	0.02	0.02	0.05	0.03
Al_2O_3	35.27	0.21	36.75	0.20	34.63	0.61
Fe_2O_3	2.26	0.09	1.20	0.07	1.54	0.07
CuO	7.98	0.16	8.16	0.14	8.71	0.46
ZnO	0.03	0.04	0.08	0.07	0.04	0.04
CaO	0.06	0.02	0.05	0.01	0.07	0.05
Na_2O	0.02	0.02	0.01	0.02	0.01	0.01
K_2O	0.04	0.01	0.04	0.01	0.03	0.01
MgO	0.01	0.01	0.01	0.01	0.01	0.01
BaO	0.08	0.04	0.05	0.04	0.07	0.04
PbO	0.03	0.03	0.03	0.04	0.03	0.04
SO_3	0.36	0.07	0.26	0.06	0.49	0.22
Total	79.77		80.96		79.44	
Structural formula based on 20 anions						
P	3.970		3.977		4.006	
Si	0.003		0.004		0.010	
Al	5.799		5.930		5.718	
Fe^{3+}	0.237		0.124		0.162	
Cu	0.836		0.839		0.915	
Zn	0.001		0.003		0.001	
Ca	0.007		0.005		0.007	
Na	0.002		0.002		0.001	
K	0.008		0.008		0.008	
Mg	0.001		0.001		0.001	
Ba	0.008		0.005		0.007	
Pb	0.004		0.004		0.004	
S	0.051		0.035		0.068	
Σ	10.927		10.937		10.909	
Cu+K+Na+Ba	0.86		0.86		0.93	
Al+ Fe^{3+}	6.04		6.05		5.88	
P+Si+S	3.98		3.99		4.03	

The treated samples show high amounts of K due to the Zachery process and stoichiometric recalculation does not match the turquoise formula (Table 2). Moreover, significant contents of Na_2O also occur linearly correlated with K_2O (Fig. 2a). In the perpendicularly cut samples (*TT_7* and *TT_8*) the highest values of K and Na are found in the darker zones, well visible to the naked eye, and at the rim where an increase of P and a decrease of Al occur; an example of *TT_8* line 2 is given in Figure 2b. In the inner parts of both samples, backscattered images evidence brighter areas enriched in CuO from 8 up to 29 wt% (an example of *TT_7* in Fig. 3 and chemical analyses in Table 3).

In *TT_9*, analyzed from rim to rim only on the polished surface, the chemical composition respects the stoichiometry of turquoise except at the rims where contents of the K and Na oxides were higher (up to 3.8 and up to 0.5 wt%, respectively).

Table 2 Representative electron microprobe analyses of treated turquoises

Sample	*TT_7 line 1*		*TT_8 line 2*				*TT_9 line 1*				
	rim	inter	rim	inter	inter	center	rim	inter	center	inter	rim
P_2O_5 (wt%)	38.18	37.14	35.44	34.15	34.29	33.59	32.41	34.16	33.98	34.23	33.39
SiO_2	0.05	0.02	0.03	0.05	0.01	0.04	0.08	0.03	0.02	-	-
Al_2O_3	24.48	27.87	28.57	30.11	31.21	31.28	32.62	34.68	34.76	35.04	34.59
Fe_2O_3	0.40	0.52	0.85	0.95	0.74	0.86	0.48	0.52	0.56	0.50	0.42
CuO	4.20	5.29	5.75	6.12	6.39	6.68	6.35	6.66	6.45	6.57	6.55
ZnO	0.02	0.03	0.21	0.18	0.32	0.21	0.05	0.03	-	0.03	0.11
CaO	0.66	0.14	0.16	0.10	0.18	0.34	0.06	0.08	0.02	0.06	0.07
Na_2O	2.14	1.61	0.88	0.70	0.53	0.30	0.50	0.25	0.20	0.22	0.36
K_2O	11.03	7.45	6.22	5.60	4.13	3.47	3.80	0.81	0.75	1.02	2.00
MgO	0.13	-	0.04	-	0.05	0.06	0.02	0.02	-	-	0.01
BaO	0.10	0.01	0.03	-	-	0.03	0.05	0.07	-	0.02	0.01
PbO	0.06	-	-	0.06	0.01	0.10	-	0.02	-	0.01	0.09
SO_3	0.12	0.21	0.15	0.30	0.21	0.21	0.30	0.35	0.33	0.26	0.28
Total	81.57	80.28	78.33	78.32	78.07	77.15	76.73	77.69	77.08	77.96	77.88
Structural formula based on 20 anions											
P	4.611	4.459	4.361	4.197	4.199	4.158	4.021	4.090	4.088	4.087	4.031
Si	0.010	0.003	0.007	0.010	0.001	0.008	0.017	0.007	0.004	-	-
Al	4.115	4.659	4.894	5.152	5.321	5.390	5.634	5.780	5.822	5.824	5.813
Fe^{3+}	0.043	0.056	0.093	0.103	0.081	0.094	0.053	0.055	0.060	0.053	0.045
Cu	0.450	0.563	0.627	0.667	0.694	0.733	0.698	0.707	0.688	0.695	0.701
Zn	0.001	0.001	0.008	0.007	0.012	0.008	0.002	0.001	-	0.001	0.004
Ca	0.071	0.015	0.018	0.011	0.020	0.038	0.007	0.009	0.002	0.007	0.008
Na	0.296	0.222	0.124	0.099	0.074	0.042	0.072	0.034	0.027	0.030	0.050
K	2.631	1.767	1.512	1.360	0.999	0.849	0.931	0.192	0.179	0.241	0.477
Mg	0.012	-	0.003	-	0.005	0.005	0.002	0.002	-	-	0.001
Ba	0.011	0.001	0.003	-	-	0.003	0.005	0.008	-	0.002	0.001
Pb	0.010	-	-	0.009	0.002	0.016	-	0.003	-	0.001	0.014
S	0.017	0.029	0.021	0.044	0.030	0.031	0.044	0.050	0.047	0.037	0.039
Σ	12.277	11.775	11.672	11.659	11.438	11.375	11.486	10.937	10.918	10.978	11.184
Cu+K+Na+Ba	3.47	2.57	2.30	2.14	1.80	1.68	1.72	0.95	0.90	0.98	1.24
Al+ Fe^{3+}	4.16	4.71	4.99	5.25	5.40	5.48	5.69	5.84	5.88	5.88	5.86
P+Si+S	4.64	4.49	4.39	4.25	4.23	4.20	4.08	4.15	4.14	4.12	4.07

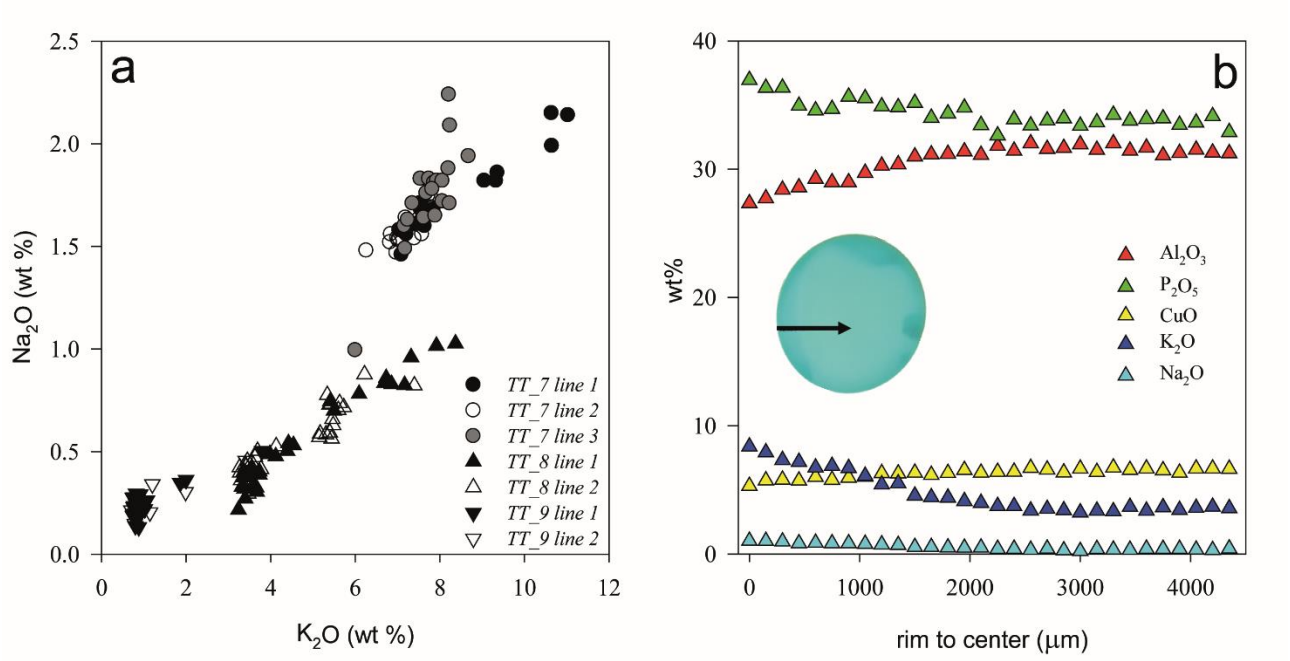

Fig. 2 a) Variation of K_2O versus Na_2O of treated samples; b) variation of different oxides in *TT_8 line 1* from rim to core

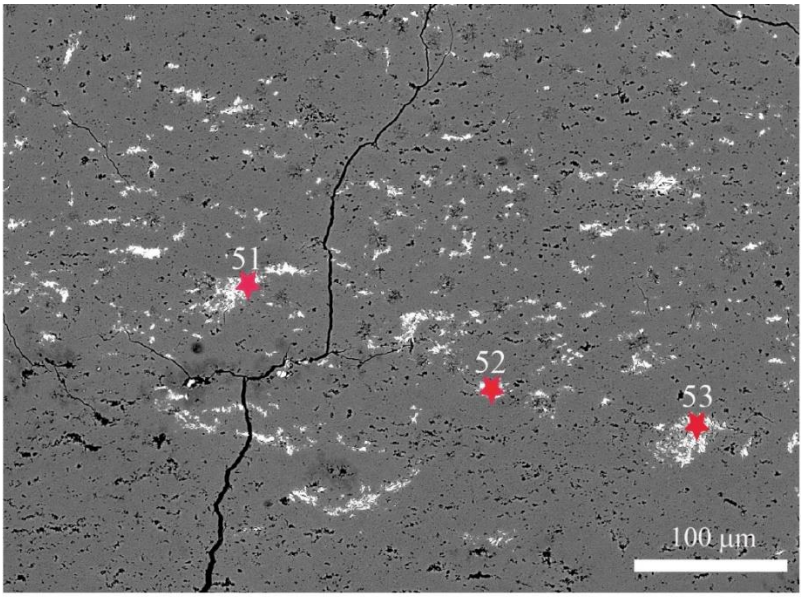

Fig. 3 BSE image of *TT_10* showing analyzed points reported in Table 3

Table 3 Electron microprobe analyses of points shown in Fig. 3

	TT_10		
wt%	51	52	53
P_2O_5	35.78	33.90	36.01
SiO_2	0.11	0.11	0.04
Al_2O_3	12.45	7.11	16.19
Fe_2O_3	0.23	0.21	0.31
CuO	24.17	28.96	19.36
ZnO	0.13	-	-
CaO	0.19	0.20	0.22
Na_2O	5.33	6.36	4.43
K_2O	5.73	4.63	6.40
MgO	-	0.02	0.03
BaO	0.02	0.08	0.08
PbO	-	-	0.03
SO_3	0.03	0.05	0.03
Total	84.16	81.63	83.12

In general, the EDS analyses of our turquoises, both natural and treated, yielded results well in the range of those from WDS-EMP. In the treated samples, the highest Cu values were detected in the more brilliant white points that contain up to 34 wt% of CuO (an example, *TT_12*, Fig. 4). The rounded crystals show a pseudo-turquoise composition with a K_2O content up to 11 wt%; the platy area shows to be composed of both pseudo-turquoise and mixed phases with variable composition containing P, Si, K, Al, Mg, Na, Cu and Fe.

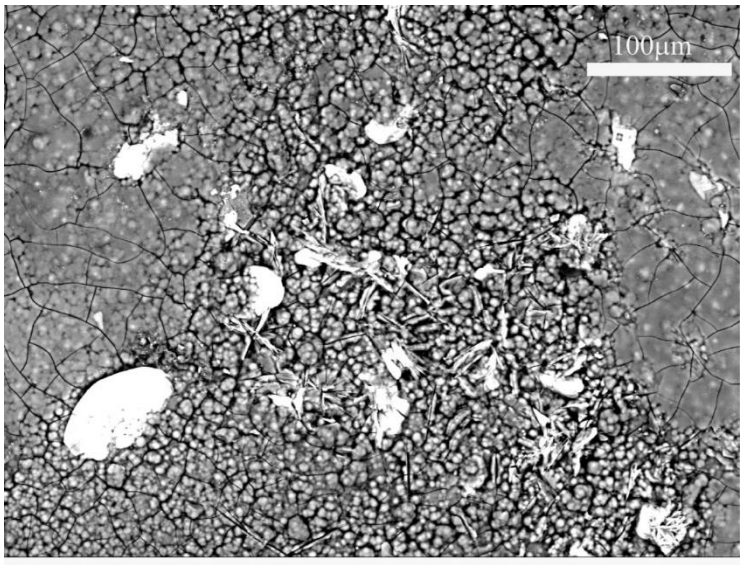

Fig. 4 BSE image of *TT_12*

In addition, the core of *TT_12* (Fig. 4) displays on the central part of the sample, the presence of K-feldspar with composition: $K_{0.98}Na_{0.03}Al_{1.0}Si_{2.93}O_8$. In Figure 5, a BSE image of the analyzed zone is displayed together with the X-

ray maps of major elements. The feldspar (black star in BSE image, Fig. 5) is in contact with "the turquoise" where a 32 wt% CuO content was detected (red star in figure).

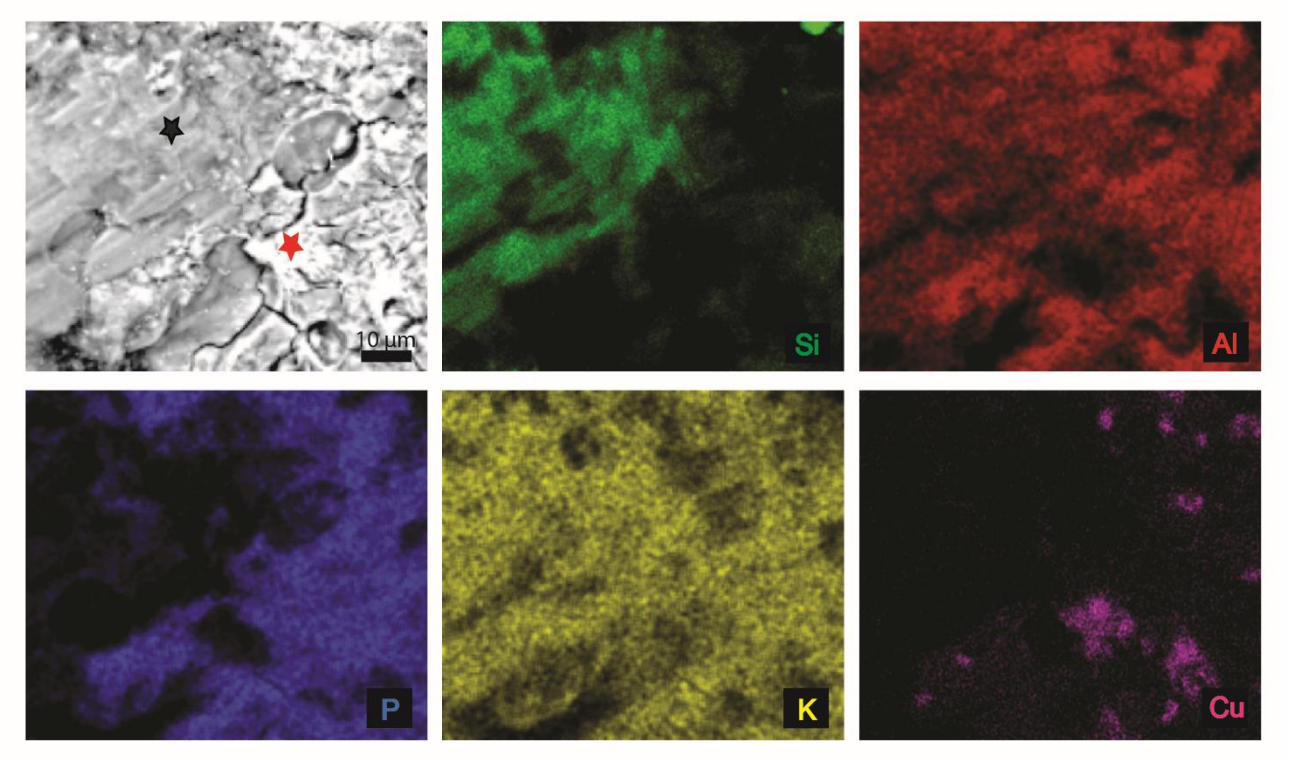

Fig. 5 BSE image and X-ray maps of selected elements of *TT_12*

An inspection at higher magnification of backscattered images evidenced white areas (Fig. 6) associated with white rounded "seeds" distributed around them (Fig. 6 a, b, c) also visible in the near platy zone (Fig. 6 d). The chemical compositions of the points labeled in Figure 6 are listed in Table 4; the copper content is very high while aluminum and potassium contents are low (point 13). Moving away, the Cu content decreases whereas that of Al and K increases.

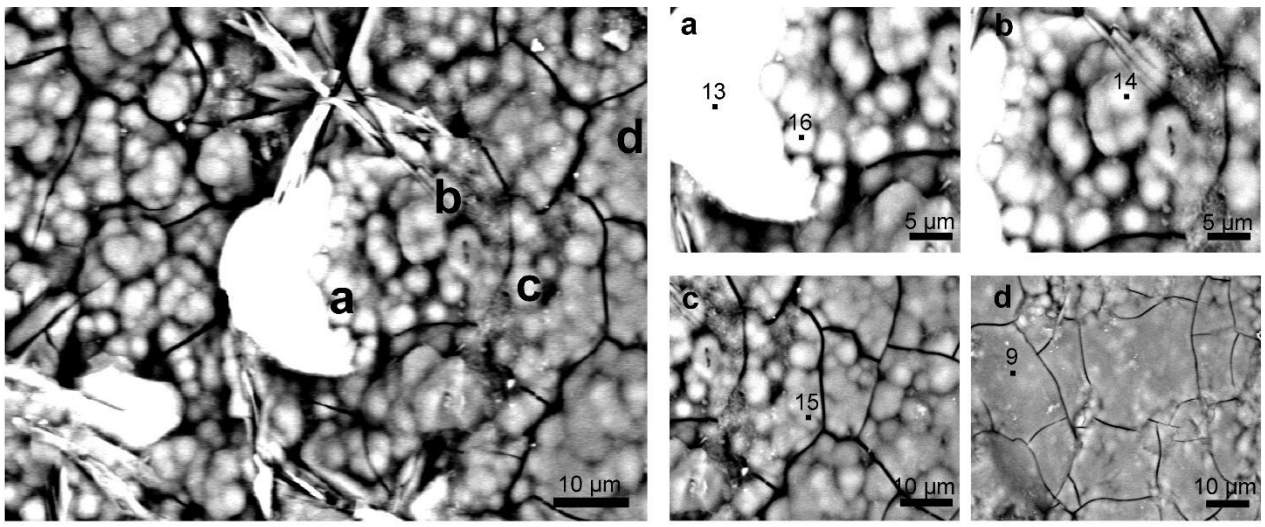

Fig. 6 BSE images of TT_12, on the left, and enlargements of the indicated a, b, c, d areas showing the analyzed points reported in Table 4, on the right.

Table 4 EDS chemical analyses of points shown in Fig. 6

	TT_12				
	13	16	14	15	9
P_2O_5 (wt%)	37.79	33.35	34.14	38.38	32.8
SiO_2	1.05	0.92	0.84	0.98	3.49
Al_2O_3	2.95	15.54	17.42	18.09	18.43
CuO	34.47	6.53	3.38	3.5	3.37
CaO	-	3.41	4.31	5.22	-
Na_2O	-	2.12	1.43	0.98	1.59
K_2O	4.7	7.81	8.49	9.58	8.66
Total	80.96	69.68	70.01	76.73	68.34

Moreover, in sample *TT_11* (Fig. 7), SE images at very high magnification of the inner part of pores allow noting the growth of crystals that are similar to those identified as turquoises by Kwon et al. (2009) in Zachery-treated stones. These Authors suggest that the crystals filling the pores influence the stability and durability of the turquoise. Unfortunately, in our sample, the gold coating prevented the EDS analysis.

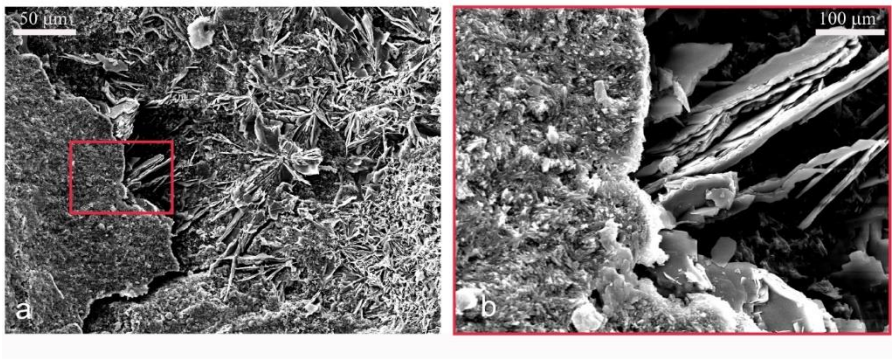

Fig. 7 a) SE images of *TT_11;* b) zooming of red rectangle in a)

X-ray powder diffraction

Figure 8 shows a comparison between the XRPD patterns of (a) natural sample *TN_12*, (b) light blue in color inner part and (c) bluest in color outer part of treated sample *TT_23*. All samples showed the characteristic diffraction pattern of turquoise even though the treated turquoise exhibits larger unit cell parameters giving rise to a slight expansion of the unit cell volume when compared to the natural ones (461.88 vs. 461.44 $Å^3$, respectively). The Rietveld analysis yields minor contents of pyrite (4 wt%) in natural sample whereas a 3 wt% of tenorite is obtained for the light blue area of the treated stones (Fig. 9).

Concerning the bluest area of the outer part of treated sample, the XRPD pattern supports the existence of an amorphous phase that is clearly displayed by a diffuse bump in the 20-30 $2\theta°$ region of the background, suggesting the occurrence of a poor to non-crystalline phase in the outer part of the treated gem. Additionally, the lower size of the diffraction domains extracted from the microstructural analysis suggests a poor crystallinity of this material occurring in the outer layer of the gem.

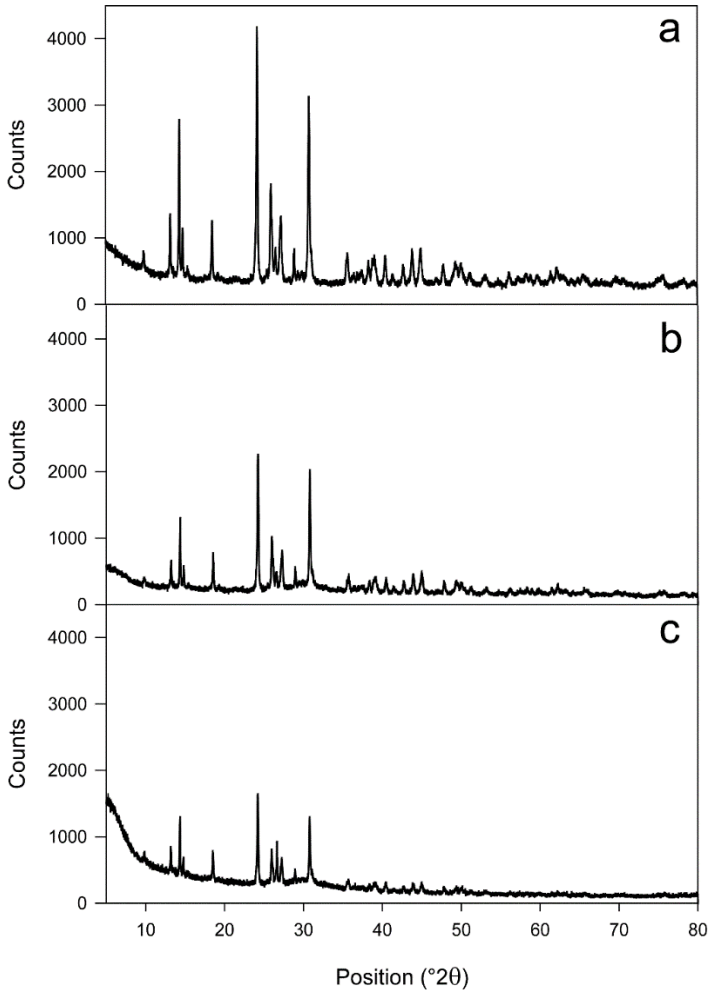

Fig 8 XRPD patterns of a) *TN_12*, b) inner and c) outer part of *TT_23*

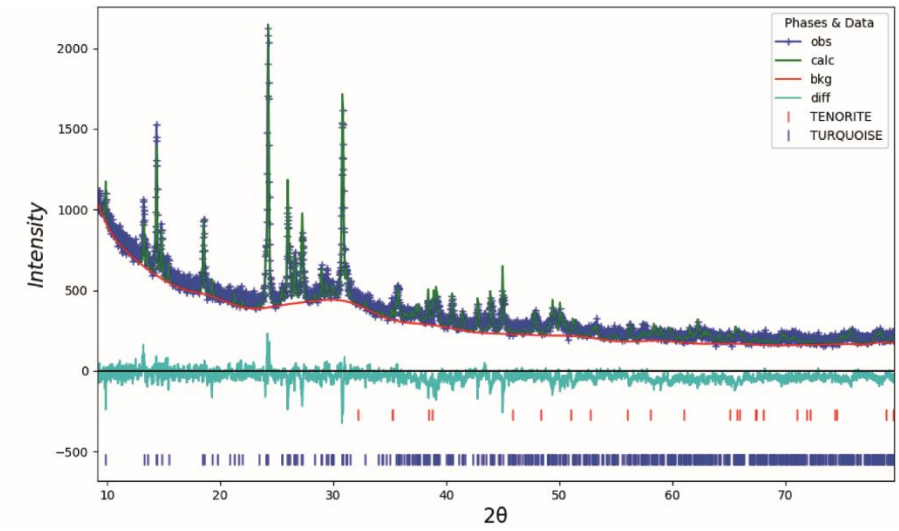

Fig. 9 Observed and calculated X-ray powder diffraction pattern after the Rietveld refinement of sample *TT_23*

Laboratory-based X-ray Computed microtomography (µCT)

The µCT analyses allowed exploring in a non-invasive way the microstructure of natural (*TN_11)* and treated (*TT_20*) gems. The former is characterized by an outer surface with micropores and microcracks leading to a whole porosity of 5

vol% (Fig. 10 a). These cracks do not show any preferred orientation and develop also in the inner part of the gem and appear filled with finely-aggregates characterized by high and low grey scale values (Fig. 10 b-c). The EMPA analyses of the same sample suggest the occurrence of clay minerals and pyrite filling the cracks.

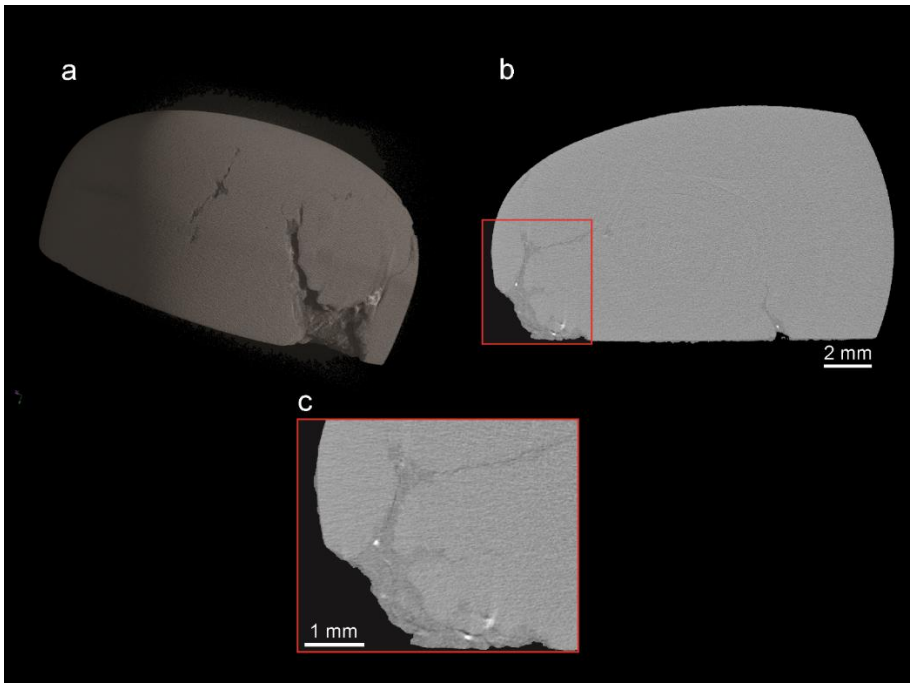

Fig. 10 Natural turquoise *TN_11*: a) 3D volume rendering (200x500x1000 voxels); b) selected sagittal reconstructed slice; c) minerals filling fractures (zooming of the red rectangle in Fig. 10 b)

In Figure 11 a, the volume rendering of the treated gem is displayed, and a reconstructed axial slice of its inner part is shown in Figure 11 b. It is clear that surface porosity observed in natural samples is now completely lost whereas the outer white circular region (*i.e.*, with highest attenuation of X-rays) appears and extends in its inner part exhibiting a concentric banding. In the core of the gem, well-rounded aggregates with a high grey scale values appear randomly dispersed and exhibit a size of ~ 20 µm (Fig. 11 c). 3D rendering of the segmented highly absorbing aggregates is shown in Figure 11 d.

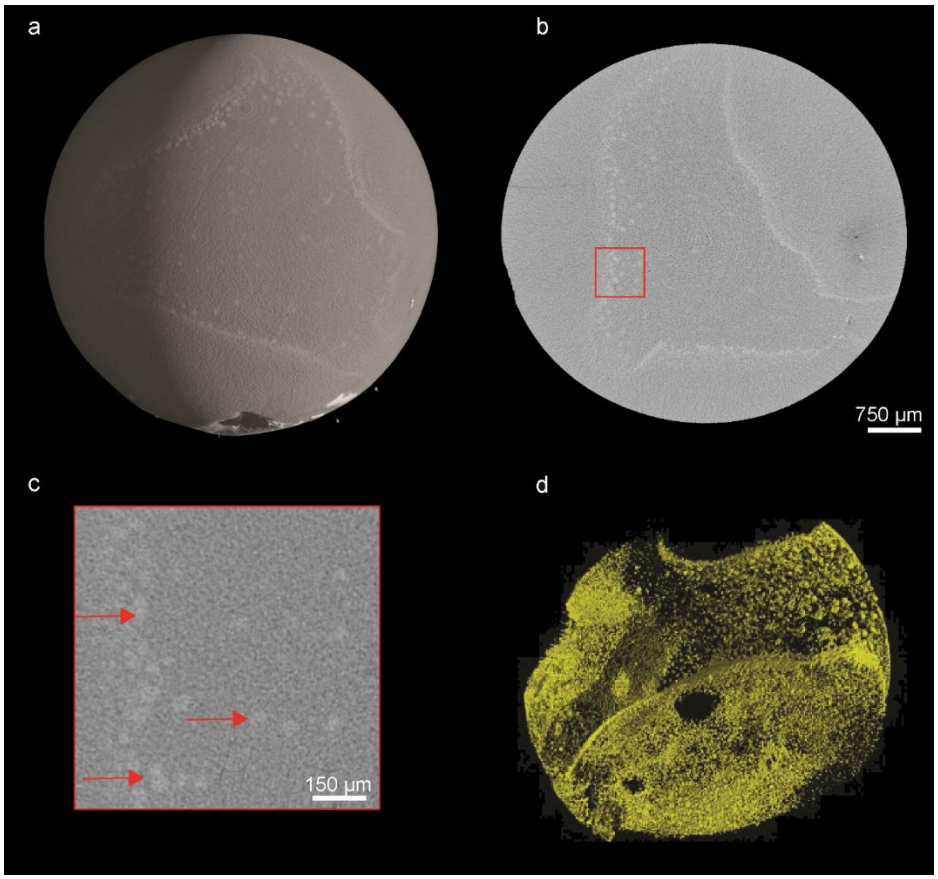

Fig. 11 Zachery tretated turquoise *TT_20*: a) 3D volume rendering (500x500x500 voxels); b) selected axial reconstructed slice; c) rounded highly X-ray attenuation aggregates (zooming of the red rectangle in fig. b); d) 3D rendering of the segmented highly absorbing aggregates

Fourier transform infrared spectroscopy

FTIR and ER-FTIR spectra of natural and treated turquoises were collected on several points and traverses from the rim to the center of the samples. It is noteworthy that FTIR requires a micro sampling, which may not be routinely carried out in the analysis of gems whereas ER-FTIR allows for a non-invasive investigation of the surface of materials, which potentially opens its use for gemological applications. As a drawback, intrinsic limitations of this last technique include the possible presence of spectral artifacts due to surface effects and the need for reference data for spectral interpretation.

Selected results are given in Figures 12 and 13. Both IR techniques show slight differences in the patterns collected on natural and treated turquoises.

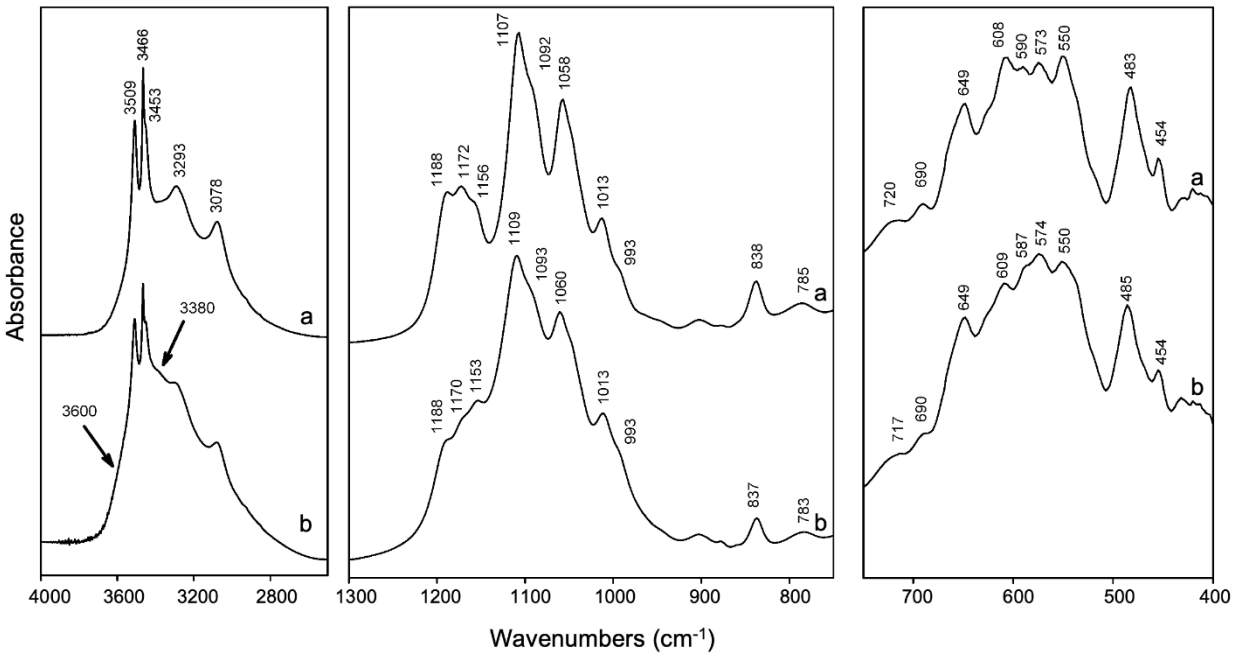

291

292 **Fig. 12** FTIR spectra collected in the different wavenumber ranges: from 4000 to 2600 cm^{-1} (left panel), from 1300 to
293 750 cm^{-1} (center panel), and from 750 to 400 cm^{-1} (right panel). a) natural *TN_14* and b) treated *TT_24* turquoise

294

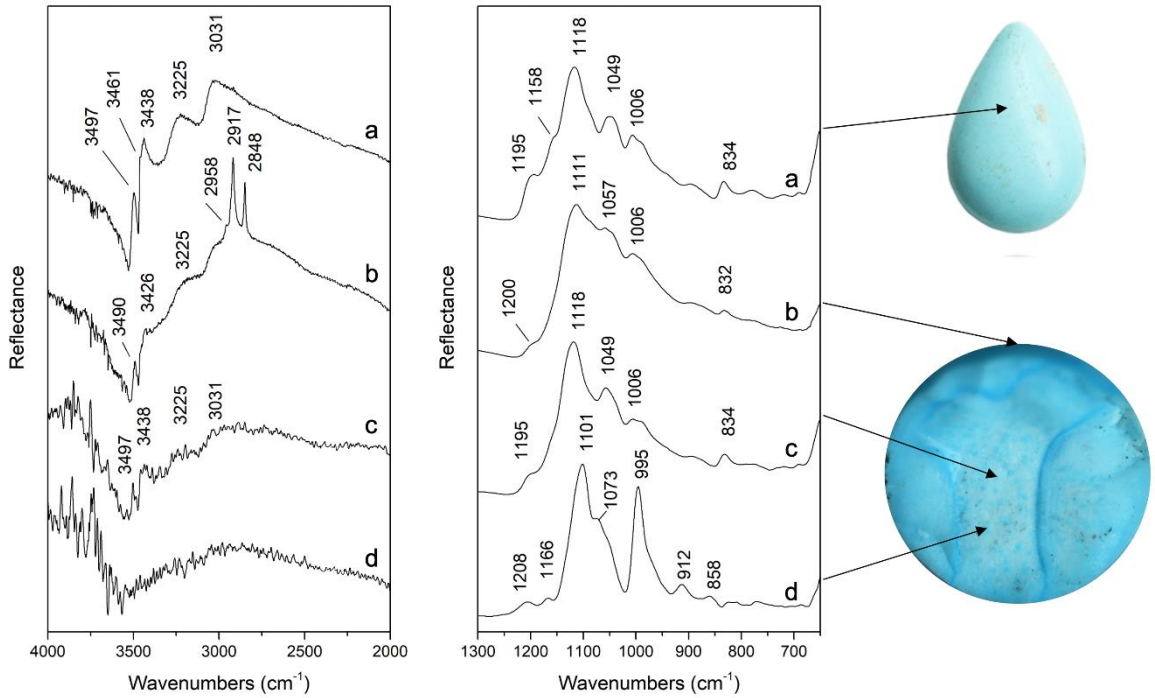

295

296 **Fig. 13** ER- FTIR spectra collected in specular geometry on different wavenumber ranges: from 4000 to 2000 cm^{-1} (left
297 panel) and from 1300 to 650 cm^{-1} (right panel). *TN_15* natural turquoise (a), *TT_20* treated turquoise in correspondence
298 of the treated surface (b), of core of the gem (c) and of the bluish internal rims and bluish crystal aggregates randomly
299 dispersed in the core of the gem (d)

300 In the water stretching region (4000-2700 cm^{-1}), the FTIR spectra of our natural untreated samples (pattern a, Fig.12)
301 show peaks at 3509, 3466, 3453, 3293 and 3078 cm^{-1} that are due the OH/H_2O vibrations (Abdu et al. 2011; Čejka et al.
302 2015), while the ER-FTIR spectra (patterns a, Fig. 13) show sharp peaks at 3497, 3461, 3438 cm^{-1} and broad bands at

3225 and 3031 cm^{-1} due to hydroxyl groups and to the two independent water units in the turquoise structure, respectively (Reddy et al. 2006; Abdu et al. 2011; Schwarzinger and Schwarzinger 2017; Sabbaghi 2018). The stretching and bending vibrations of PO_4 units are located between 1200 and 400 cm^{-1}. The main bands are found at 1107, 1058, 608, and 550 cm^{-1} in the FTIR spectra (pattern a, Fig. 12) and at 1118, 1049 and 1006 cm^{-1} and 834 cm^{-1} in the ER-FTIR ones in Fig. 13, pattern a (Fritch et al. 1999). These FTIR and ER-FTIR spectral features are well distinctive of crystalline natural turquoise.

At least two new components at about 3380 cm^{-1} and 3600 cm^{-1} appear in the FTIR spectra of treated samples (arrowed in pattern b of *TT_24* as an example, Fig. 12); the former strongly overlaps with the 3280 cm^{-1} broad component, while the latter appears as a strong asymmetry of the 3509 cm^{-1} band. Slight modifications of the FTIR patterns are also visible in the range of PO_4 antisymmetric stretching modes (1200-1000 cm^{-1}: Ross 1974; Della Ventura et al. 2019), where shifts and broadening of the 1188-1160 cm^{-1} peaks are observed in treated turquoises (pattern b of *TT_24* as an example, Fig. 12).

Differences in terms of relative intensities, position and width of bands are clearly visible in the ER-FTIR spectra of treated turquoises. In particular, the OH/H_2O stretching bands of structural water appear weaker and less defined than in the ER-FTIR spectra of natural ones (pattern b, Fig.13). The bands in the PO_4 stretching region are broader, the main peak of turquoise shifts from 1118 to 1111 cm^{-1}, and some bands (*i.e.*, at 1158 cm^{-1}) disappear whereas the bands at 2958, 2917 and 2848 cm^{-1} ($–CH_2$ and $–CH_3$ stretching vibrations) (pattern b, Fig. 13) are due to wax used to polish the surface of the treated turquoise (Han et al. 2015).
In the core of the treated gems, the possible structural/compositional variations are less evident and the ER-FTIR spectra resemble those of the untreated natural well-crystalline turquoise (*e.g.*, pattern c, Fig.13).
A completely different vibrational pattern is obtained in correspondence of the internal rims and of crystal aggregates randomly dispersed in the core of the gem already analyzed by micro-tomography *TT_20* (the same particles having a high grey scale values and micrometric size in the micro-CT analyses of Fig. 9). In these regions (see pattern d, Fig. 13), strong reflectance peaks at 1101, 1073, 995 cm^{-1} and weaker peaks at 1208, 1166, 912, 858 cm^{-1} are due to an unidentified crystalline phase. This spectrum is compatible with that of a hydroxide (maybe a potassium-containing phase) and/or of alumina (Schroeder 2002; Hosseini et al. 2011; Hong et al. 2016; Schwarzinger and Schwarzinger 2017; Sabbaghi 2018) but further investigations in reflectance mode on mineral references would be needed for its/their unambiguous identification.

Discussion and conclusions

In this study, a multidisciplinary approach offers significant novel insight into the undisclosed property Zachery treatment on turquoise. The comparison between natural and treated turquoise allows identifying, for the first time, new chemical-mineralogical and microstructural features, which are distinctive of the Zachery treatment and will be hereafter discussed.

- ✓ Chemical analyses performed by EMPA on treated samples confirmed the presence of K as already reported in literature (Fritsch et al. 1999; Kwon et al. 2009; Sun et al. 2014) but pointed out new diagnostic chemical features for the treatment. The quantitative analysis by WDS highlights a variable composition overall in terms of minor oxides (mainly K and Na) in the treated turquoises that do not respect its stoichiometric formula. This suggests

that a newly formed phase (*"transitional phase"*, see below), with a chemical composition close to the one of turquoise but not attributable to one of the six end members of its isostructural series (Abdu et al, 2011), is the resulting product of the Zachery treatment. At present, no crystalline phases with a chemical composition matching with the one calculated are available in the literature.

The presence of K in treated samples well agrees with the hypothesis of Frisch et al. (1999) suggesting that turquoise grows in situ within the porous areas during the treatment process. The involvement of potassium in the formation of turquoise is also described in the recent paper on the Ali Abad Cu Porphyry Deposit in central Iran, by Ardekani et al. (2020). The Authors suggest that the presence of potassium in some analyses of turquoises probably indicates the presence of a *transitional phase* resulting from the conversion of sericite or alunite to turquoise and they report a series of reactions under acid conditions involving sulfates, phosphates, and potassium (released from the alteration of feldspars) finally bearing to the crystallization of turquoise;

- ✓ BSE images and EDS analyses highlight scattered spots yielded very high copper concentration up to 34 wt% CuO in the inner part of the treated turquoise and suggest that these Cu-rich areas are micro spheres ("seeds") that decrease in size and in copper content moving from the inner core to the outer part of the gem;

- ✓ EDS and XRPD analyses of treated samples highlighted the occurrence of K-feldspar and tenorite. The former should represent a relict of the "beds of feldspar" used during the Zachery process while the latter (CuO) can be interpreted as the product of the oxidation of copper sulfides added in the soaking process. We might suppose in the Zachery treatment the use of chemicals such as copper sulfate for the enhancement of turquoise. As noticed for chalcedony by Koivula and Kammerling (1989), man-made "inclusions" may be produced by soaking porous samples in a copper solution and then applying an electric current to precipitate out a dendrite of elemental copper;

- ✓ The XRPD patterns suggest that the outer surface of the treated turquoise is characterised by the coexistence of a crystalline phase, namely turquoise, with an amorphous/poorly crystalline phase (probably the transitional phase and/or the residues of the products used in the treatment). Furthermore, the structural refinement of the turquoise on the gem surface indicates a lower crystallinity. The hypothesis is that the Zachery treatment induces the re-crystallization of a new turquoise which differs from the natural one from a microstructural point of view;

- ✓ X-ray computed microtomography allows investigating both the outer and inner part of the gem in a totally non-invasive way; the effects of the Zackery treatment are clearly observable not only on the surface but also in its inner core. Concentric banding associated with well-rounded aggregates (CuO seeds) extend from the inner to the outer surface. Furthermore, the enhancement due to the treatment resulted in a lowering of the value of porosity in treated samples which may justify the darker surface color of treated samples;

- ✓ The spectral differences detected by the two infrared techniques (FTIR and ER-FTIR) suggest the occurrence of a possible structural and/or compositional slight variations between natural and treated turquoise, thus confirming the XRPD results. This spectral modification is detectable on the external surface of treated turquoises as well as in the subsurface regions of the treated gem (as showed by ER-FTIR spectra collected on the internal rims of cross-sectioned samples) and suggests a surface-bulk gradient of the effects induced by the Zachery method.

In conclusion, we might assert that the combination of several analytical techniques allows for the complete characterization of natural and treated turquoise, thus providing (i) new chemical and structural features, which are

peculiar of the Zachery treatment and (ii) new insights of this turquoise treatment. In particular, the non-destructive ER-FTIR spectroscopy and microtomography allow distinguishing, in a fast and easy way, between natural and Zachery-treated samples whereas invasive EMPA-EDS and XRPD can provide information on the treatment process.

Acknowledgement The authors gratefully thank Claudio Cimmino, Bangkok, Thailandia for providing the samples here investigated, Giada Marchetti for collecting part of the experimental data during her degree and Ludovica Faldi (IGI Milan) for acquiring the gem photos.

Declarations

The authors did not receive support from any organization for the submitted work.

The authors have no relevant financial or non-financial interests to disclose.

Competing Interests

The authors declare no competing interests.

Author Contributions: V.D., N.M. and R.B. wrote the main manuscript text. V.D. performed the EMP analysis and interpreted the results. E.P., N.M. and G.D.V. performed the FT-IR analysis and elaborated the data. N.M. and M.C. performed XRPD and elaborated the data. I.A. performed the gemological analyses. L.M. performed the X-ray computed micro-tomography analysis and L.M. and N.M. elaborated the data. All authors assisted in the revision of the initial draft of the manuscript.

References

Abdu YA, Hull SK, Fayek M, Hawthorne FC (2011) The turquoise-chalcosiderite $Cu(AlFe^{3+})_6(PO_4)_4(OH)_8 \cdot 4H_2O$ solid-solution series: A Mössbauer spectroscopy, XRD, EMPA, and FTIR study. Am Mineral 96:1433-1442. https://doi.org/10.2138/am.2011.3658

Ardekani SJ, Mackizadeh MA, Ayati F (2020) Mineralogy and Formation Conditions of Turquoise in Ali Abad Cu Porphyry Deposit. J Econ Geol 12(1): 93-109. https://doi: 10.22067/econg.v12i1.72122

Carò F, Schorsch D, Smieska L, Santarelli B (2021) Non-invasive XRF analysis of ancient Egyptian and near Eastern turquoise: A pilot study. Archaeol Sci Rep 36: 102893**.** https://doi.org/10.1016/j.jasrep.2021.102893

Caruso V, Marinoni N, Diella V, Berna F, Cantaluppi M, Mancini L, Trombino L, Cattaneo C, Pastero L, Pavese A (2020) Bone diagenesis in archaeological and contemporary human remains: an investigation of bone 3D microstructure and minero-chemical assessment. Archaeol Anthropol Sci 12: 1-18. https://doi.org/10.1007/s12520-020-01090-6

Čejka J, Sejkora J, Macek I, Malikova R, Wang L, Scholz R, Xi Y, Frost RL (2015) Raman and infrared spectroscopic study of turquoise minerals. Spect Acta Part A: Molecular and Biomolecular Spect 149: 173-182. https://doi.org/10.1016/j.saa.2015.04.029

Della Ventura G, Capitelli F, Capitani G, Ventruti G, Monno A (2019) X-ray structure refinement and vibrational spectroscopy of metaxauxite $FeAl_2(PO_4)_2(OH)_2 \cdot 8H_2O$. Crystals 9, 297: 1-14. https://doi.org/10.3390/cryst9060297

Dumanska-Slowik M, Wesełucha-Birczyńska A, Natkaniec-Nowak L, Gaweł L, Włodek A (2020) blue or green? Turquoise-planerite species from Carico Lake Valley in Nevada, the United States: Evidence from Raman spectroscopy. J Raman Spectrosc 51: 346-356. https://doi.org/10.1002/jrs.5761

Feldkamp LA, Davis LC, Kress JW (1984) Practical cone-beam algorithm. J Opt Soc Am A 1: 612–619. https://doi.org/10.1364/JOSAA.1.000612

Fritsch E, Mcclure SF, Ostrooumov M, Andres Y, Moses T, Koivula JI, Kammerling RC (1999) The identification of Zachery-treated turquoise. Gems Gemol 35: 4-16

Fritsch E, Rondeau B (2009) Gemology: the developing science of gems. Elements 5: 147-152. https://doi.org/10.2113/gselements.5.3.147

Hainschwang T, Notari F (2008) Specular reflectance infrared spectroscopy – a review and update of a little exploited method for gem identification. J Gemmol 31: 23-29

Han W, Lu T, Dai H, Su J, Dai H (2015) Impregnated and dyed turquoise. Gems Gemol 51: 343-345

Hole F, Flannery KV, Neely JA (1969) Prehistory and Human Ecology of the Deh Luran Plain: An Early Village Sequence from Khuzistan, Iran. University of Michigan Press. http: //dx.doi.org/10.3998/mpub.11395036

Hong Z, Li J, Jiang J, Li Z, Xu R (2016) Competition between bacteria and phosphate for adsorption sites on gibbsite: An in-situ ATR-FTIR spectroscopic and macroscopic study. Colloids Surfaces B: Biointerfaces 148: 496–502. https://doi.org/10.1016/j.colsurfb.2016.09.026

Hosseini SA, Niaei A, Salari D (2011) Production of γ-Al_2O_3 from Kaolin. Open J Phys Chem 1: 23-27. http:// doi.org/10.4236/ojpc.2011.12004

Koivula JI, Kammerling RC (1989) Gems News. Gems Gemol 25: 45-51

Kudrna Prašek M, Pistone M, Baker DR, Sodini N, Marinoni N, Lanzafame G, Mancini L (2018) A compact and flexible induction furnace for in situ X-ray microradiograhy and computed microtomography at Elettra: design, characterization and first tests. J Synchrotron Rad 25 (4), 1172-1181. https://doi.org/10.1107/S1600577518005970

Kwon KR, Bang SY, Park JW, Shim KB (2009) Structural characteristics of Zachery-treated turquoise. J Korean Cry Growth and Cry Tech 19: 95-101

Lind T, Schmetzer K, Bank H (1983) The identification of turquoise by infrared spectroscopy and X-ray powder diffraction. Gems Gemol 19: 164-168

Mancini L, Dreossi D, Fava C, Sodini N, Tromba G (2007) TomoLab: the new X-ray micro-tomography facility at Elettra. Elettra Highlights 2006-2007

McClure SF, Kane RE, Sturman N. (2010) Gemstones enhancement and its detection in the 2000s. Gems Gemol 46: 218-240

Reddy BJ, Frost RL, Weier ML, Martens WN (2006) Ultraviolet-Visible, near Infrared and Mid Infrared Reflectance Spectroscopy of Turquoise. J. Near Infr Spectr 14: 241–250. https://doi.org/10.1255/jnirs.641

Rietveld HM (1969) A profile refinement method for nuclear and magnetic structures. J App Cryst 2**:** 65-71

Ross, S.D. (1974) Phosphates and other oxy-anions of group V. In Mineralogical Society Monograph 4: The Infrared Spectra of Minerals; Farmer, V.C., Ed.; Mineralogical Society of Great Britain and Ireland: Twickenham, UK

Sabbaghi HA (2018) A combinative technique to recognise and discriminate turquoise stone. Vib Spec 99: 93-99. http://doi.org/10.1016/j.vibspec.2018.09.002

Schindelin J, Arganda-Carreras I, Frise E et al (2012) Fiji: an open-source platform for biological-image analysis Nat. Methods 9:676-682. https://doi.org/10.1038/nmeth.2019

Schroeder PA (2002) Infrared Spectroscopy in Clay Science. In: Rule A, Guggenheim S (eds) CMS Workshop Lectures. Teaching Clay Science 11: 181–206. https://doi.org/10.1346/CMS-WLS-11.11

Schwarzinger B, Schwarzinger C (2017) Investigation of turquoise imitations and treatment with analytical pyrolysis and infrared spectroscopy. J Anal Appl Pyrolysis 125: 24-31. http://doi.org/10.1016/j.jaap.2017.05.002

Shigley JE, McClure SF (2009) Laboratory-Treated Gemstones. Elements 5: 175-178.
http://doi.org/10.2113/gselements.5.3.175
Sun LH, Ling A, Yu F, He Z, Ma W (2014) A tentative discussion on Zachery-treated turquoise. Acta Petr Miner 33: 165-171 (in Chinese, abstract in English)
Toby BH, Dreele RB (2013) GSAS-II: the genesis of a modern open-source all purpose crystallography software package. J App Cryst 46: 544-549. https://doi.org/10.1107/S002188981300353
Zandomeneghi D, Voltolini M, Mancini L, Brun F, Dreossi D and Polacci M (2010) Quantitative analysis of X-ray microtomography images of geomaterials: application to volcanic rocks. Geosphere 6: 793-804.
https://doi.org/10.1130/GES00561.1